1*H*-Azepine-2-oxo-5-amino-5-carboxylic Acid: a 3_{10} Helix Inducer and an Effective Tool for Functionalized Gold-Nanoparticles

Sara Pellegrino †, Andrea Bonetti †, Francesca Clerici †, Alessandro Contini †, Alessandro Moretto§, Raffaella Soave ‡, and Maria Luisa Gelmi †*

*e-mail: sara.pellegrino@unimi.it

† Università degli Studi di Milano-DISFARM-Sez. Chimica Generale e Organica "A.Marchesini"-via Venezian 21-20133-Milano-Italy

§ Università degli Studi di Padova-Dipartimento di Scienze Chimiche- via Marzolo 1- 35131 Padova- Italy

‡ CNR- Istituto di Scienze e Tecnologie Molecolari-Via Golgi 19 - 20133 Milano-Italy.

KEYWORDS: alpha,alpha disubstituted amino acids, functionalized gold nanoparticles, 3_{10} helix, peptidomimetics

ABSTRACT

A new α,α-disubstituted constrained glutamine analogue was designed to decorate gold-nanoparticles and to induce 3_{10}-helix when inserted in peptides. Using an efficient "one-pot"

asymmetric Schmidt reaction, between 4-disubstituted-cyclohexanone and hydroxyalkylazides, 1*H*-azepine-2-oxo-5-amino-5-carboxylic acid, (**oxo-Azn**) was prepared. The main (*R*) isomer was inserted at the *N*-terminus in a very short peptide sequence, *i.e.* PhCO-(R)-Oxo-Azn-L-Ala-Aib-L-AlaNHMe and a stable 3_{10}-helix conformation was obtained, as verified by both NMR experiments and molecular dynamics (MD) simulations. Finally, the presence of the hydroxyl chain at nitrogen atom of the ring allowed the preparation of covered chiral gold nanoparticles.

Introduction

Small molecules functionalized gold nanoparticles (GNPs) are at the forefront of the research in nano chemistry.[1] The three dimensional self-assembled monolayers constructed by the introduction of organic compounds on GNPs have emerged as versatile tools of surface modification. Furthermore, the organic monolayer reduces the surface energy of GNPs and thus provides increased solubility and colloidal stability.[2]

Amino acids and peptides are effective building blocks to create hierarchical nanomaterials [3] and functionalized GNPs. [4] They feature a multitude of functionalities and unique secondary structures based on controllable primary sequences and environmental conditions.[5] By using amino acids and peptides, it is thus possible to tailor new hybrid materials for a broad range of applications in different areas, such as medicine, bionanotechnology, and electrochemistry.[6] On the other hand, focusing on biomedical applications, the peptide instability toward proteases might be a concern. Synthetic analogs of natural amino acids represent valuable tools to overcome this problem.[3b,7] In particular, the use of α,α-disubstituted derivatives gives the double advantage of reducing the metabolic degradation, and of stabilizing the helical conformation, by reducing the available conformational space of the peptide backbone.[8]

Continuing our researches on unnatural constrained amino acids, [9] we, recently, prepared a α,α-disubstituted ornithine analogue, *i.e.* 1*H*-azepine-4-amino-4-carboxylic acid (Azn), as an effective 3_{10}-helix inducer.[9c] Reasoning on the possibility to use this scaffold as the key material to decorate gold nanoparticles, we designed, a α,α-disubstituted cyclic glutamine analogue, *i.e.* 1*H*-azepine-2-oxo-5-amino-5-carboxylic acid, named Oxo-Azn, containing on the nitrogen side chain a hydroxy tethering group (Figure 1).

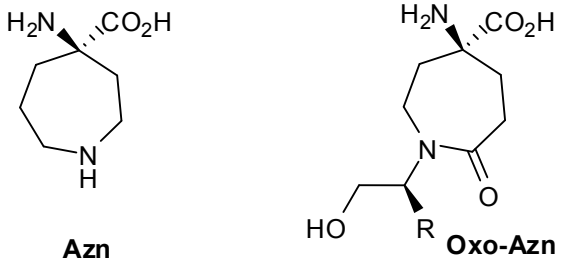

Figure 1. Chemical structures of **Azn** and **Oxo-Azn**

Oxo-Azn was prepared using a very efficient one-step asymmetric Schmidt reaction that gives a mixture of "quasi enantiomers", easily separated by chromatography (Scheme 1). The main (*R*) isomer was thus inserted at the *N*-terminus in a very short peptide sequence, *i.e.* PhCO-(R)-Oxo-Azn-L-Ala-Aib-L-AlaNHMe. A stable 3_{10}-helix conformation was obtained, as verified by both NMR experiments and molecular dynamics (MD) simulations. Finally, taking advantage of the tethering group, covered chiral gold nanoparticles have been prepared and fully characterized.

RESULTS AND DISCUSSION

Synthesis of Oxo-Azn scaffold. 1*H*-azepine-2-oxo-5-amino-5-carboxylic derivatives **5/6** were synthesized through an asymmetric Schmidt reaction[10] on cyclohexanone **1**[9c] and benzyl or phenyl substituted hydroxyalkylazides (**2a,b**) (Scheme 1) The reaction was performed in CH_2Cl_2 and in the presence of an excess of $BF_3{\cdot}OEt_2$ (from -80 to 25 °C). After 48 h, the reaction was quenched with 2N NaOH affording a mixture of "quasi enantiomers" **5** and **6** (**5a/6a**: 67:33, 80%; **5b/6b**: 50:50, 75%; ^{1}H NMR and HPLC analyses). A similar diastereoselection and yield were obtained by changing the temperature (from -10 to 25 °C) and the reaction time (18 h).

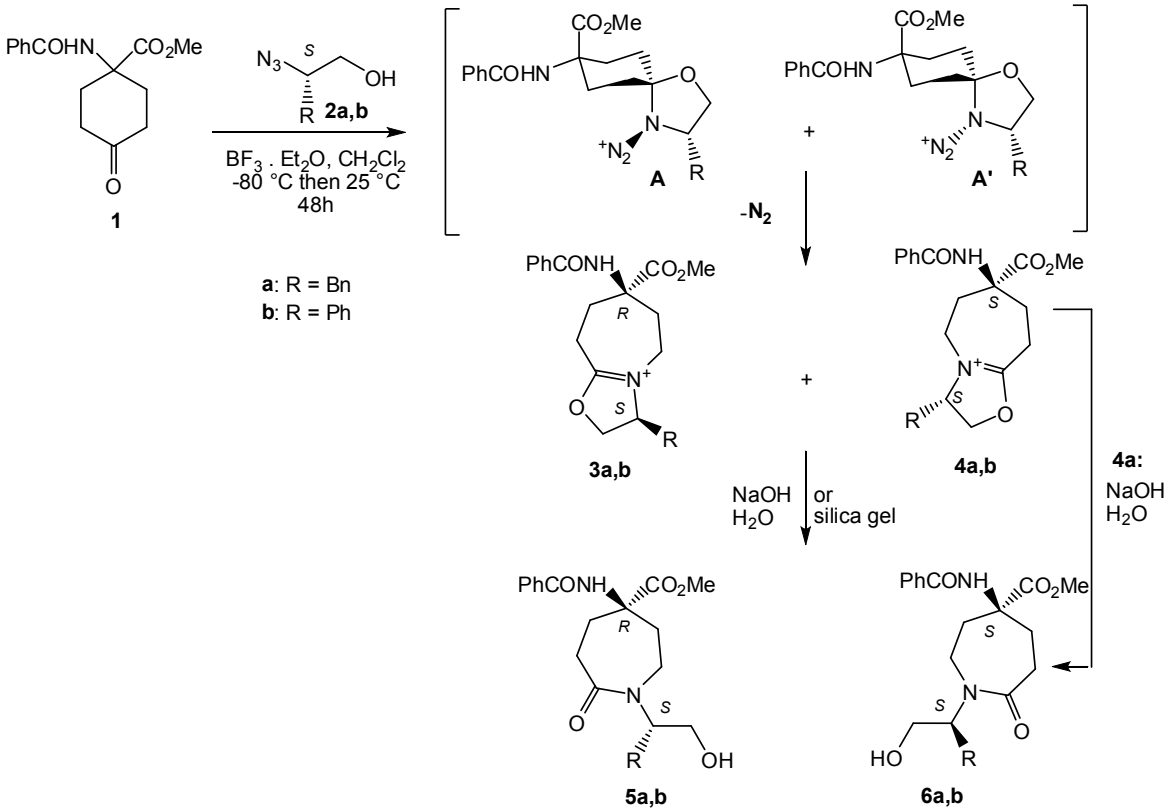

Scheme 1. Asymmetric Schmidt reaction on ketone **1**.

To gain insight on the mechanism and diastereoselection, the reaction between **1** and **2a** was monitored by ^{1}H NMR. After 18 h, ^{1}H NMR analysis of the crude, before NaOH quenching, showed the formation of intermediates **3a**/**4a** in 67:33 ratio. This mixture was crystallized from Et_2O affording the pure bicyclic intermediate **4a** (13%). Pure azepinone derivatives **5a** (45%) and **6a** (10%) were isolated after column chromatography of the mother liquors. (Scheme 2).

Finally, the treatment of **4a** with NaOH (2N, 24 °C, 30 min.) gave the minor stereoisomer **6a** in quantitative yield (Scheme 1). X-Ray of the single crystal of **4a** (Figure 2) allowed to assign unequivocally the stereochemistry of each adduct (for NMR discussion see Supporting Information).

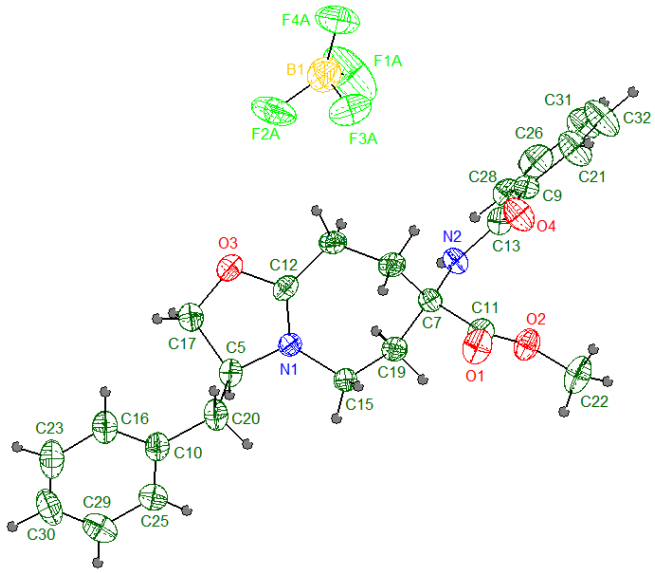

Figure 2. ORTEP plot of **4a** at 293 K with atom numbering scheme; ellipsoids of non-H atoms at 30% probability level.

The isolation of the rigid bicyclic intermediate **4a** allowed to confirm that the mechanism of formation of "quasi enantiomers" **5/6** is the one proposed by Aubè et al. [10] Accordingly, the azidoaddition occurs on ketone **1** possessing the chair conformation bearing the amido group in the equatorial position (confirmed as the most stable by theoretical calculations). In this way a couple of diastereoisomeric spiro intermediates **A** and **A'** that differ for the stereochemistry of nitrogen leaving group, is formed. Consequently to the departing of N_2, the antiperiplanar migration of the

methylene group of cyclohexyl ring occurs affording, from **A**, bicyclic salt **3**, and from **A'**, salt **4** (Scheme 1).

Although the reaction occurred via the same mechanism, we found a different distribution of the diastereomers, with respect to literature data on 4-mono-substituted cyclohexanones. As an example-[10a] the Schmidt reaction between 4-*tert*-butylcyclohexanone and azide **2b** leads to the S diastereoselection through the stabilization of intermediate **A'** by cation-π interaction. In our case, using the same azide, no diastereoselection was observed, suggesting that steric factors drive the diastereoselction outcome. This hypothesis is confirmed by the partial diastereoselection found in the case of azide **2a**, containing the more flexible benzyl substituent. In this case, the minimization of steric interactions between the nitrogen leaving group and the benzyl substituent favours the formation of intermediate **3a** with respect to **4a**.

Synthesis of tetrapeptide PhCO-(R)-Oxo-Azn-L-Ala-Aib-L-AlaNHMe. The model peptide PhCO-(*R*)-Oxo-Azn-L-Ala-Aib-L-AlaNHMe was then prepared starting from α,α-amino acid **5a** (Scheme 2). The sequence Ala-Aib-Ala has been deeply investigated in the literature, using both experimental techniques (NMR, CD, X-ray) and MD.[11] In all studies, it has been emerged that multiple conformations are present, and that it is necessary to increase the length of the peptide chain to obtain stable helical conformations. Regarding **Oxo-Azn**, *R*-isomer was selected since it is known that only the *R*-**Azn** isomer, (see Figure 1), is able to induce a 3_{10}-helix when inserted in a short pentapeptide containing L-amino acids.[9c]

In order to have in hand the necessary quantity of scaffold **5a** for the peptide synthesis' optimization, the reaction between ketone **1** and azide **2a** was scaled up to 11g of **1**, yielding **5a** in 47% yield after column chromatography purification. The ester function on scaffold **5a** was hydrolyzed using a methanolic solution of NaOH (2N) in CH_2Cl_2/MeOH (9:1, 25 °C, 15h). Acid **7** was isolated in 95% yield. Compound **7** was made to react with alanine benzyl ester *p*-toluenesulfonate [HOAt (1 equiv.)/EDC (1 equiv.)/DIPEA (2 equiv.), CH_2Cl_2 25 °C, 2 h] affording dipeptide **8** (58% yield). The yield of **8** were increased (80%) using the free amine derivative of alanine operating with the same condensative conditions (15h). The benzyl group of the ester function was removed by hydrogenolysis (Pd/C, MeOH, 25 °C, 24h) giving acid **9** (90%, Scheme 3). The final tetrapeptide **10** (50%) was obtained by reaction of **9** with dipeptide H_2N-Aib-*L*-Ala-CONHMe [HOAt (1equiv.)/EDC (1equiv.)/DIPEA(2 equiv.), CH_2Cl_2 25 °C, 15 h]. It has to be underlined that in these

reaction conditions the epimerization of the alanine stereocenter was not observed (HPLC analysis, Figure S4 in the Supporting Information). Any attempt to synthesized directly compound **10** from **5a** and H_2N-*L*-Ala-Aib-*L*-Ala-CONHMe tripeptide failed, probably for the steric hindrance on the carboxylic function of **7**.

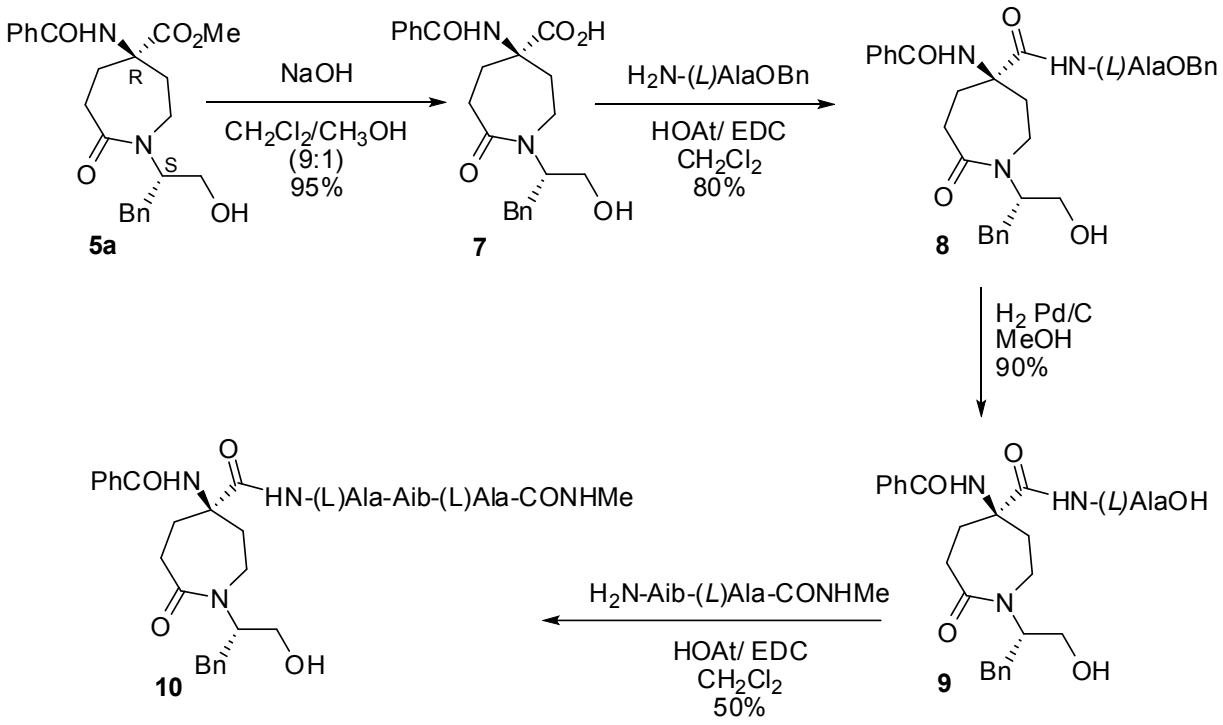

Scheme 2. Synthesis of tetrapeptide PhCO-(*R*)-Oxo-Azn-L-Ala-Aib-L-AlaNHMe

Tetrapeptide **10** was first purified by preparative RP-HPLC. During the purification we observed the formation of a by-product, corresponding to the bicyclic derivative **11** (Figure 3; see supporting information for NMR discussion). Its formation must be ascribed to the TFA present in the RP-HPLC eluent phases that catalysed the oxazoline ring formation. To overcome this issue, compound **10** was directly purified by crystallization (CH_2Cl_2/Et_2O) of the crude reaction mixture.

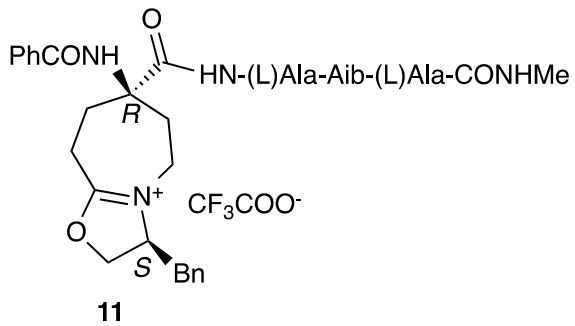

Figure 3. Chemical structure of **11**, the product of transformation of **10** in acidic conditions

*NMR conformational studies on model peptide **10**.* A full assignment of the protons of peptide **10** was accomplished by 500 MHz NMR analysis (1H, ^{13}C, COSY, TOXY and HSQC NMR experiments, see Supporting Information). 2D-NOESY at different mixing times and temperature-dependent chemical shift variation experiments (from 273 to 333 K) were performed in CD_3CN solution, to obtain detailed information on the conformational behavior of **10**.

A complete set of N,N (i,i + 1) NOE cross-peaks [PhCONH/Ala-2 (w); Ala-2/Aib (m); Aib/Ala-4(vs)] were detected excepting for Ala-4/MeNH that are overlapped (Figure 4A).

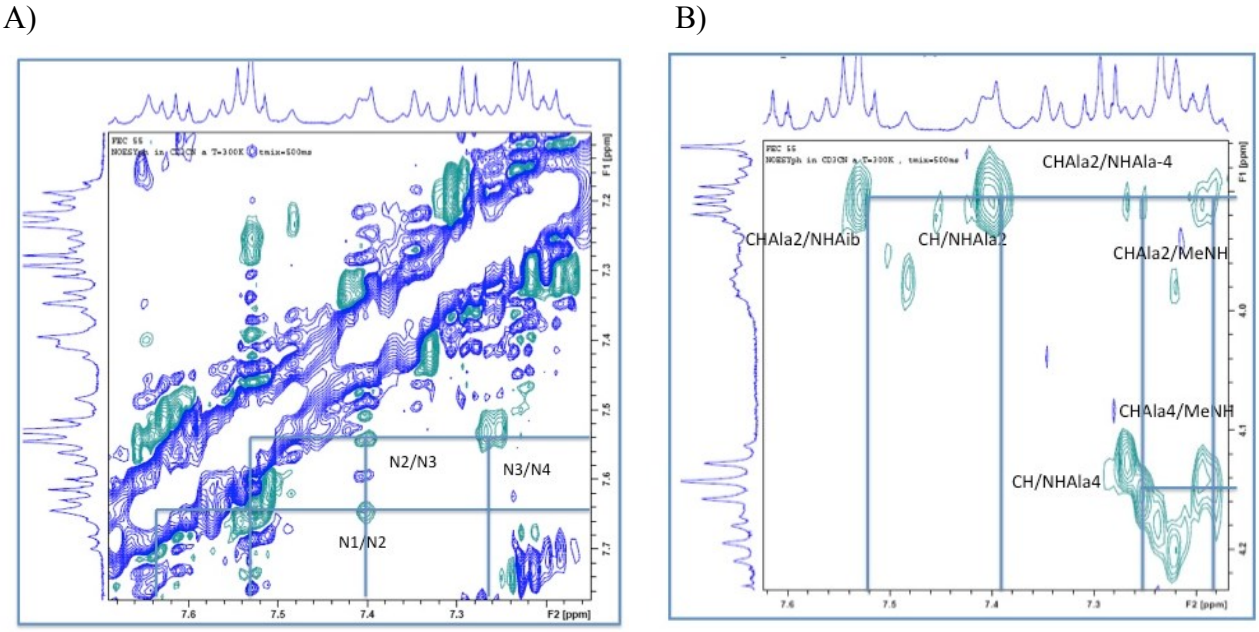

Figure 4. Sections of the NOESYspectrum of **10** (10.2 mM CD_3CN solution, 500 MHz, 25 °C, 500 ms mixing time): A) NH/NH and B) α-H/NH N.o.e. regions.

Various NOEs are operative in the peptide chain, *i. e.* α,N (i,i+1) between Ala-2/Aib (m), and Ala-4/NHMe (w). (Figure 4B) Longer range α,N (i,i+2) and α,N (i,i+4)NOEs allow to define the helix types: the former is typical of a 3_{10}-helix, while the latter is typical of an α-helix.[9c] In our case, of relevance, are the long range N.o.e of Ala-2/Ala-4 [α,N(i,i+2; w), (Figure 4B) and of the phenyl ring of benzyl moiety (δ 7.94) and the methyl of Aib (δ 1.54, m) (Figure 5). A further long range Noesy was detected between Ala-2 and NHMe [α,N(i,i+3; m)]. All these data are in agreement with a 3_{10}-helix conformation.

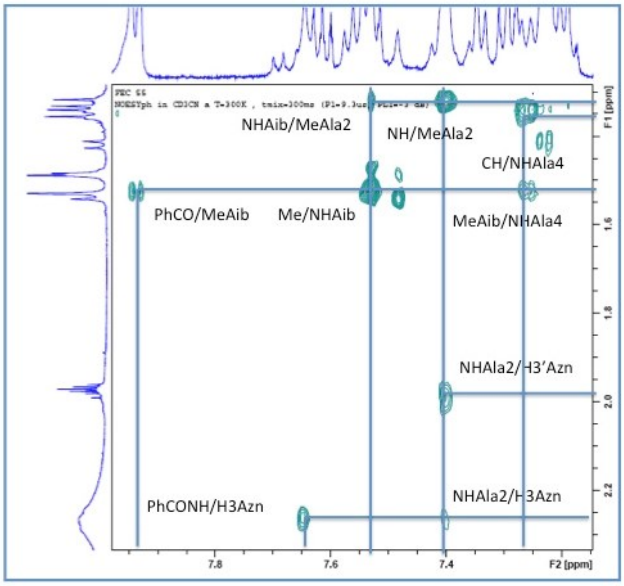

Figure 5. Section of the NOESYspectrum of **10** (10.2 mM CD_3CN solution, 500 MHz, 25 °C, 300 ms mixing time): NH/β-H N.o.e. region.

^{13}C values of the anysotropic Me of Aib that are in a magnetically inequivalent environment such as in a helix structure, differ of more than 2 ppm.[11a] In our case δ ^{13}C values of 23.0 and 26.4 were found for Aib-Me groups. NH chemical shifts temperature dependences, providing information on inaccessible or intramolecular H-bonds[9c] confirmed the helix structure, too. Values of -3.98 ppb K^{-1} for Oxo-Azn, -3.99 ppb K^{-1} for Ala-2, -2.57 ppb K^{-1} for Aib, -1.55 ppb K^{-1} for Ala-4 and -2.64 ppb K^{-1} for NHMe were detected (Figure 6).

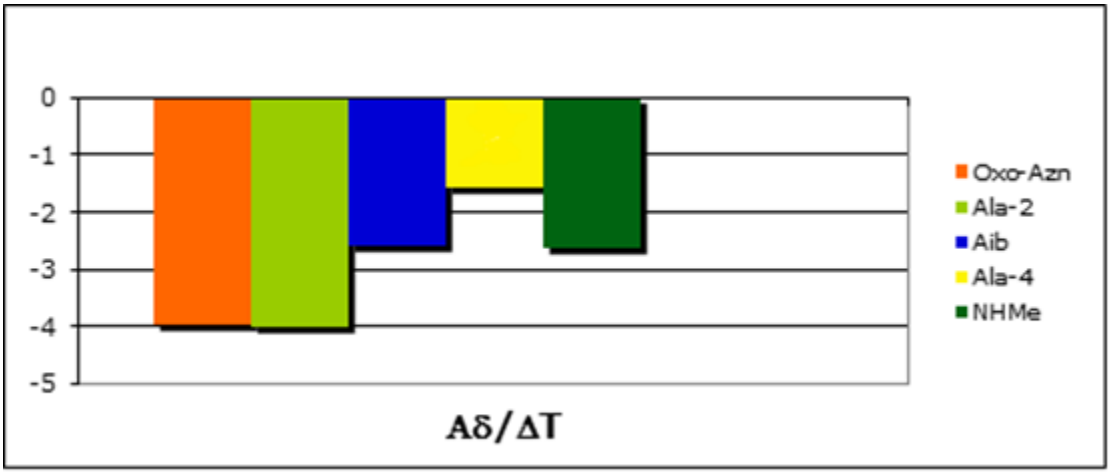

Figure 6. Temperature dependence of the NH proton chemical shifts of compound **10**.

These data suggest that NH of Aib, Ala-4, and NHMe fall within the typical ranges for intramolecularly H- bonded protons. Conversely, an equilibrium between an intramolecularly H-bonded and a non-H-bonded state is suggested for the NH of PhCONH and Ala-2 on the basis of temperature dependences (about 4 ppb K^{-1}, Figure 6).

From these findings we can postulate that a regular 3_{10}-helix construct, stabilized by three consecutive, $i + 3 \rightarrow i$ N-H···O=C intramolecular H-bonds (NH-3/PhCO, NH-4/ OxoAznCO, and NHMe/ Ala2CO) was formed. On the other hand, differently to similar compounds reported in the literature[12], we did not detect any intramolecular H-bond between the CO group of the lactame function and the NH of peptide chain that could compete in the helix formation. Therefore, it has to be stressed the ability of Oxo-Azn to strongly stabilize 3_{10}-helix even if in very short peptides.

*Molecular Dynamics (MD) studies on model peptide **10.*** To evaluate the folding behavior of (R)-Oxo-Azn, we also performed Replica Exchange Molecular Dynamics (REMD) simulations starting from a fully extended conformation of peptide **10** (φ = ψ = ω = 180°), according to the protocol reported in our previous studies.[8a,9c,9h] The resulting trajectory, extracted from each replica in order to simulate a constant temperature of 308.5 K, was then analyzed in terms of H-bonds, secondary structure and cluster analyses (Tables 1-3, Figure 7).

Table 1. Results of DSSP analysis[a] of the 100 ns REMD trajectory obtained at T = 308.53 K

#Residue	3_{10}-helix	α-helix	Turn
Oxo-Azn1	31.1	3.6	19.7
Ala2	34.7	3.6	25.8
Aib3	34.7	3.6	31.5
Ala4	18.7	3.6	30.0

[a] Values are reported as a percentage of the total secondary structures populations. The difference to 100% is the percentage of unordered secondary structure.

Table 2. Results of H-Bond analysis of the 50-100 ns REMD trajectory at T = 308.53 K

Acceptor	Donor	Occ%	AvgDist[a] (Å)	AvgAng[b] (deg.)
Ph C=O	Aib3 NH	37.0	3.20	163.1
Ala2 C=O	NHMe	27.0	3.13	160.5
oxo-Azn1 C=O	Ala4 NH	19.1	3.32	162.0
oxo-Azn1 C=O	NHMe	5.3	3.13	161.9
Ph C=O	Ala4 NH	3.9	3.42	162.9

[a]Donor-acceptor distance; cutoff = 4.0 Å. [b]Donor-H-acceptor angle; cutoff = 150 deg.

Table 3. Average dihedrals obtained from the analysis of the three most populated cluster trajectory

	#1	#2	#3	#4	#5
φ1	-29±35	15±43	22±41	-16±43	33±29
ψ1	-33±35	18±47	23±47	-20±43	35±32
φ2	-60±26	-87±48	-93±40	-64±41	35±44
ψ2	-22±19	111±81	132±69	4±46	32±17
φ3	-45±13	-22±38	40±19	22±38	46±9
ψ3	-44±29	-24±55	27±63	7±72	43±16
φ4	-85±27	-87±35	-75±60	-87±44	-78±55
ψ4	16±65	49.±81	87±86	80±91	70±92

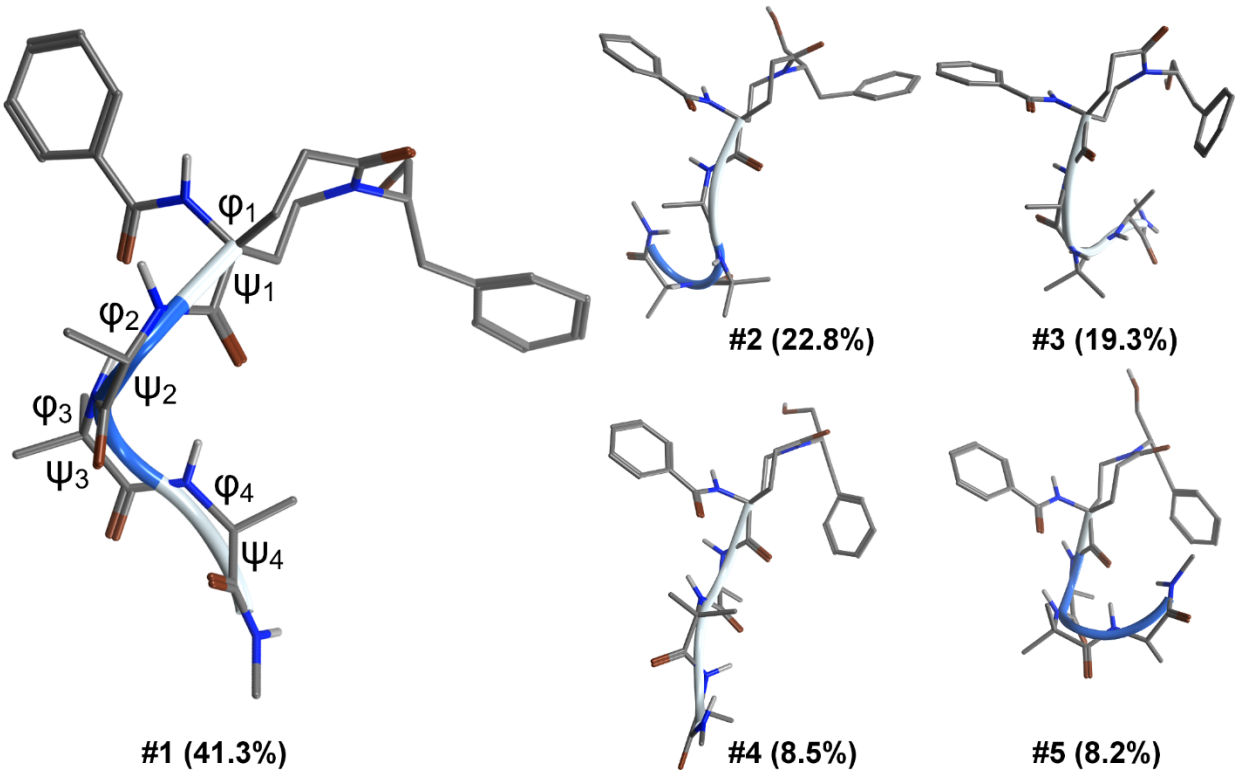

Figure 7. Representative structure and relative population (%) of the most populated clusters obtained by cluster analysis of the 50-100ns REMD trajectory obtained at T = 308.53 K

Results show that Oxo-Azn has an helical propensity similar to that observed for the parent **Azn**[8a,9c] suggesting that neither the lactame C=O nor the substituted chain at the nitrogen azepino negatively affect the ability to stabilize helical conformations. Indeed, the DSSP analysis of the REMD 308.53 K (Table1) trajectory shows a relatively high helical content for residues 1-3, with turn content being prevalent only for the C-terminal residue Ala4. It can also be observed that the helical content is principally due to 3_{10} helix conformation, with only a marginal contribution of α-helix. This is also confirmed by H-bond analysis (Table 2), since relevant H-bonds are those of the i → i+3 type (Ph C=O···HN Aib3, Oxo-Azn C=O···HN Ala4 and Ala2 C=O···HNMe), typical of 3_{10} helices, while i → i+4 H-bonds show occupancies of about 5%. Finally, geometrical clusterization (Figure 8) followed by the analysis of relevant φ and ψ dihedrals (Table 3) showed an helical conformation as the well-defined secondary structure most frequently sampled during the simulation (cluster #1, pop% = 41.3, Figure 7), even if structures classifiable as different folding intermediates (clusters #2-5) represent about 60% of the whole conformational population. By observing the average φ and

ψ values of the most populated cluster #1, it can be observed that most dihedrals fall within the range typical of 3_{10} helix (even if an α-helix cannot be excluded, if deviations from the average values are considered).[13] Further details on the folding preferences of peptide **10** were also provided by the analysis of the 3D Ramachandran plot derived from the 100 ns REMD trajectory obtained at 308.53 K (Figure 8).

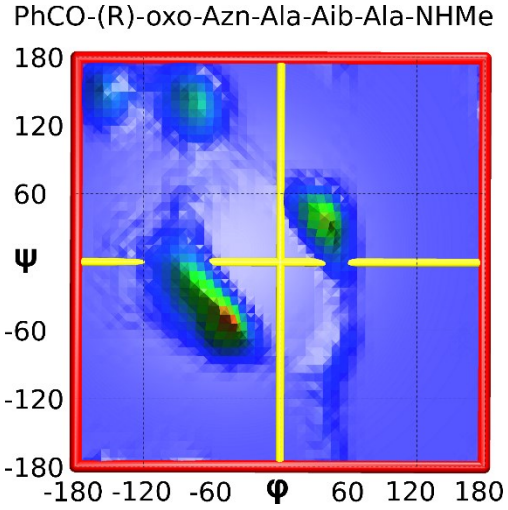

Figure 8. 3D Ramachandran plot obtained from the 100 ns REMD trajectory (308.53 K) of peptide **10**. The z-axis represents the frequency of occurrence.

It can be observed that the most frequently sampled couple of φ and ψ dihedrals is that typical of the right-handed helix secondary structure, followed by a not negligible amount of left handed helix. Dihedral values belonging to the β regions are also sampled and, interestingly, the paths connecting the different regions of the 3D-Ramachandran plot can also be observed as ruffles on the graph surface, which indicate high energy conformations which are only occasionally sampled.

*Use of scaffold **5** for gold nanoparticles preparation.* Finally, we investigated the possibility of using scaffold **5** for the obtainment of covered gold nanoparticles.

First, we introduced a thiol tether through an ester linkage with the hydroxy function of scaffold **5**. 3-Tritylsulfanyl-propionic acid was condensed with scaffold **5** using DCC and DMAP (CH_2Cl_2, 25 °C, h) affording compound **12** (80%, Scheme 3).

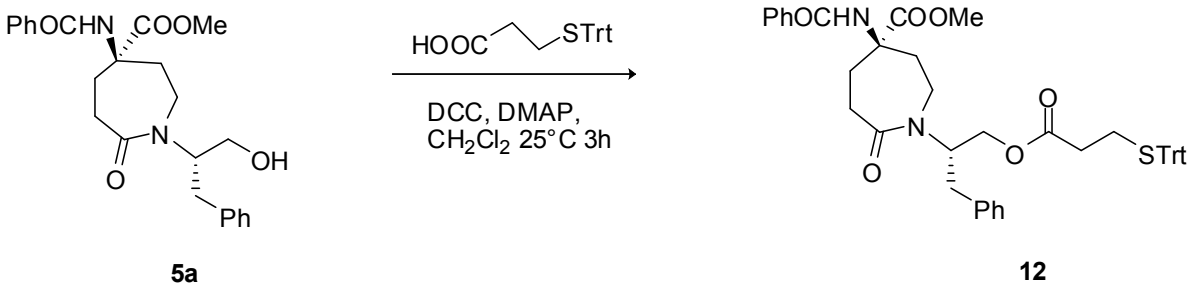

Scheme 3. Condensation between **5a** and 3-tritylsulfanyl propionic acid.

Gold nanoparticles (AuNp) were prepared by chemical reduction (with $NaBH_4$) in a methanol/water mixture of the corresponding tetrachlorohydrate salts in the presence of the amino acid conjugate **12**.[6b] The resulting dark-brown nanoparticle conjugated were found well soluble in organic solvents as CH_2Cl_2 and $CHCl_3$. Transmission electron microscopy analysis (TEM) revealed the formation of AuNp-**12** conjugated with a metallic core average diameter of 1.8 nm (Figure 9A and B, respectively). Moreover, termogravimetric analysis (TGA) showed a 55% weight loss, which is to attributed to the organic part of the cluster, thus to confirm the effective incorporation of **12** over the nanoparticle surface (Figure 9C).

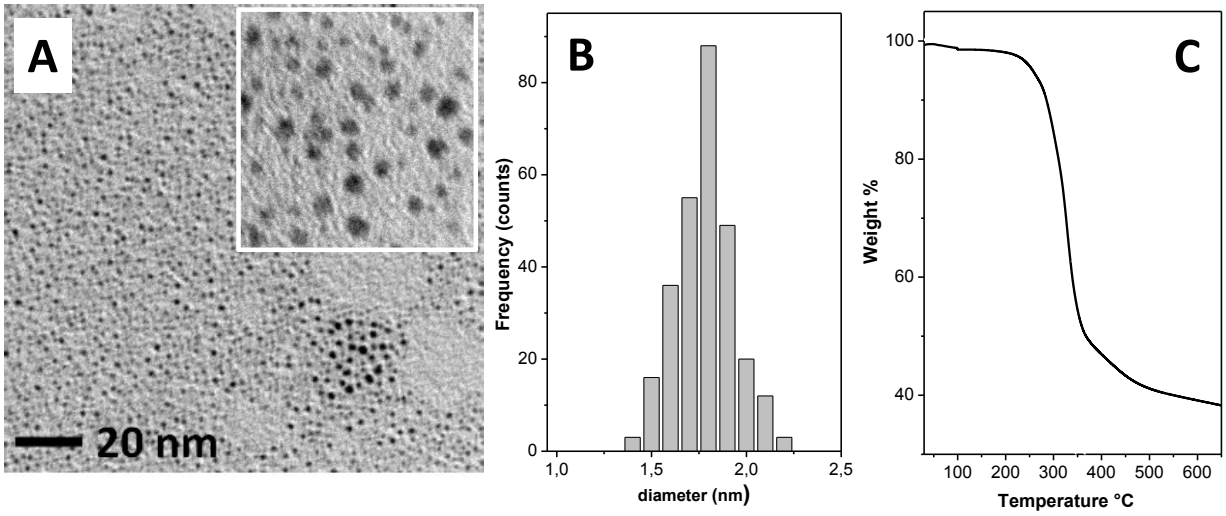

Figure 9. A) TEM image showing the formation of AuNp-**12** conjugated. Insert, detailed view of the AuNp-**12** conjugated. B) AuNp-**12** conjugated size distribution graph showing an average diameter of 1.8 nm. C) TGA analysis of AuNp-**12** conjugated showing a 55% of weight loss to be referred to the organic part of the cluster.

Furthermore, UV-Vis absorption spectra and dynamics light scattering (DLS), both recorded in CH_2Cl_2 solution, supported the formation of such nanoparticles (Figure 10A and B respectively). In particular, UV-Vis absorption spectra showed a continue absorption profile in the 300-700 absorption region, and this finding is typical for gold nanoparticle with diameter size below 2 nm.[14] Dynamic light scattering (DLS) analysis revealed 5 nm particle size distribution, which are in according with the bulky nature of the ligand. Moreover, IR (KBr) analysis showed typical amide bond signals [*v*: 3297 (NH-amides), 1734 (CO esters), 1651 (CO amide I), 1546 (CO amide II) cm^{-1}] that confirmed the occurrence of AuNp-**12** conjugation by showing the preservation of the functional groups of **5a** after its link to the gold core.

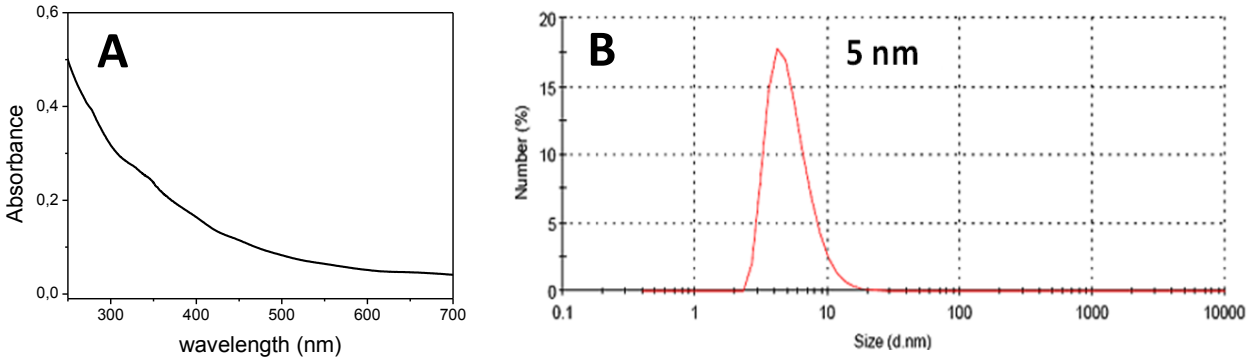

Figure 10. A) UV-Vis absorption spectra in CH_2Cl_2 solution of AuNp-**12** conjugated. B) DLS distribution of AuNp-**12** conjugated recorded in a CH_2Cl_2 solution.

Interestingly, AuNp-**12** presents a dichroic spectrum in the 350-680 nm region (Figure 11), which can be attributed to the gold core. In particular, the CD spectrum of AuNp-**12** showed two positive bands located at 300 (intense) and 500 (broad) nm, while at 400 nm displayed a weak negative band. Similar findings were reported in literature, and attributed to metal-chiral ligands interactions[15] that enhanced the intrinsic chirality of the Au core.[16]

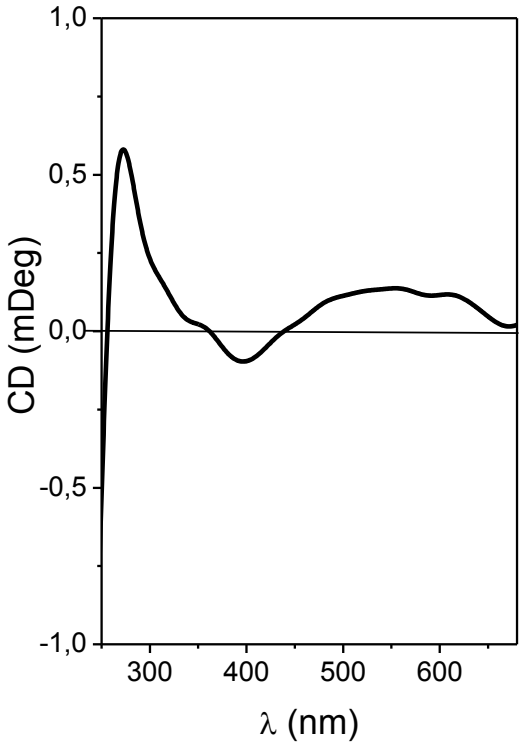

Figure 11. CD spectrum of AuNps **12** in dioxane at 20 °C in the 250-680 nm region.

Finally, by combining information from TEM and TGA analyses we may propose a structural information of AuNp-**12** conjugated, that result in a chemical formula of $Au_{201}L_{60}$.

In conclusion, the new glutamine analogue **oxo-Azn** functionalized on the nitrogen side chain with a hydroxyalkyl tether was efficiently synthesized in enantiopure form and in gram scale by an asymmetric one-step procedure. Both theoretical and dynamic NMR studies revealed that *R*-**oxo-Azn** is a good 3_{10}-helix inducer when inserted at the *N*-terminus in short peptide sequence. Finally, the presence of the tethering group allowed the preparation of covered chiral gold nanoparticles. Considering the above-mentioned helical stabilization of **oxo-Azn** in solution, it will be noteworthy in the future to deeply investigate if this ability is maintained also when linked to gold nanoparticles.

EXPERIMENTAL SECTION

The materials and solvents were purchased from common commercial sources and used without additional purification. ^{1}H NMR spectra were recorded at 200, 400 or 500 MHz and ^{13}C NMR spectra at 50, 70 or 125 MHz using TMS as internal standard. The following abbreviations were used to describe peak patterns where appropriate: singlet (s), doublet (d), triplet (t), multiplet (m), broad resonances (br). Coupling constants (*J*) are reported in Hertz. Mass spectra were recorded under electron spray interface (ESI) conditions.I nfrared spectra were recorded on a FTIR spectrometer. $[\alpha]_D$ Values were measured using $CHCl_3$ as the solvent, if not differently reported. UV-Vis absorption spectra were measured in water on a UV-Vis spectrophotometer with 1 cm path length quartz cuvettes. Samples for transmission electron microscopy (TEM) were prepared before use, by 100-fold dilution of a 2mg/ml water solution of the AuNp. A glow discharged carbon coated grid was floated on a small drop of solution and excess was removed by #50 hardened filter paper. Thermogravimetric analysis (TGA) was run on 5 mg nanoparticle samples from 25 to 1200 °C under a continuous N2 flow.

Theoretical calculations. The charge parameterization of the unnatural oxo-Azn amino acid has been performed as previously reported.[8a, 9c] Briefly, the oxo-Azn structure was designed with MOE,[17] capped with an acetyl (Ac) and a NHMe group at the N- and C-termini, respectively, and submitted to a conformational search with MOE using the following setup: Low Mode MD, MMFF94x force field, Born solvation, iteration limit = 40000, MM iteration limit = 2500, rejection limit = 500. The two lowest energy conformations having φ and ψ dihedrals matching a right- or a left-handed helix (φ = ±60°, ψ = ±45°) were selected for charge parameterization with R.E.D.IV.[18] The geometries were than optimized at the HF/6-31G(d) level and two different spatial orientations were used to derive RESP-A1 charges. Charge restraints of −0.4157, 0.2719, 0.5973 and −0.5679

were imposed to the backbone nitrogen, hydrogen, carbonyl carbon and oxygen, respectively, accordingly to the Amber *ff99SB* force field.[19]

REMD simulations were carried out on model peptide **10** by starting from an extended conformation (ψ=φ=ω= 180°) and by following a previously reported protocol, [8a, 9c] which is hereafter summarized: 12 replicas were run for 100 ns at temperatures from 260.00 to 658.94 K, using the *pmemd* module of Amber14,[20] and selecting the *ff99SB* force field coupled with the GB-OBC(II) implicit solvent model.[21] The trajectories were extracted at 308.53 K and the simulation convergence was assessed on the basis of cluster analyses performed with *cpptraj*[20]at 25-50, 50-75 and 75-100 ns time intervals. The simulations resulted fully converged already at 50 ns, and the subsequent H-bond and clustering analyses were then conducted on the 50-100 ns interval. H-bonds were analyzed with VMD 1.9.1,[22] with a donor−acceptor distance threshold of 4.0 Å and an angle cutoff of 30°. Secondary structure analyses were performed on the whole trajectory by using the DSSP method,[23] as implemented in *cpptraj*.

General Procedure for the Schmidt Reaction. *Method A)* Ketone **1**[9c] (11g, 40 mmol) was dissolved in dry CH_2Cl_2 (300 mL) under nitrogen atmosphere. After cooling at -10°C, $BF_3(OEt)_2$ (26.5 mL, 200 mmol) was dropped and the mixture was stand for 30 min after which azide **2a** or **2b** (1.3 equiv.), dissolved in CH_2Cl_2 (200 mL), was added. The stirring was continued (TLC: CH_2Cl_2/MeOH, 10:1) and the temperature was gradually increased to 25°C in 18h period. A solution of NaOH (2N, until pH 14) was added and the mixture was stirred for 30 min.. A white solid, corresponding to the isomer **6**, was formed and filtered. The organic layer was separated and the aqueous one was extracted with CH_2Cl_2 (3 x 50 mL). The organic layers were washed with a saturated solution of NH_4Cl (pH 4). After drying over Na_2SO_4 and solvent evaporation, the crude mixture was chromatographed on silica gel affording diastereoisomers **5** and **6**. *Method B)*. The reaction of azide **2a** (275 mg, 1.3 mmol) and ketone **1** (300 mg, 1.1 mmol) was performed according to point *a)* but avoiding the quenching with NaOH. After solvent evaporation, ^{1}H NMR analysis of the crude mixture showed the formation of a mixture of **3a/4a** in 67:33. The reaction mixture was taken up with Et_2O affording pure compound **4a** (60 mg, 13%), that was collected by filtration. The

mother liquors were chromatographed (CH_2Cl_2/MeOH, from 100:0 to 50:1) affording **5a** (210 mg, 45%) and **6a** (50mg, 10%).

Methyl 5-Benzoylamino-1-[(*S*)-1-hydroxy-3-phenylpropan-2-yl]-2-oxoazepan-5-carboxylate (5a/6a): 67:33. Column chromatoghraphy condition:CH_2Cl_2/MeOH, from 100:0 to 10:1

(*R*)-**5a**: 8.5 g, 47%. Mp 234 °C (CH_2Cl_2/MeOH); $[\alpha]_D^{25}$ -24.7 (*c* 0.2, DMSO); IR (KBr) ν_{max} 3340, 1723, 1660 cm^{-1}; ^1H NMR (DMSO-d_6, 500 MHz) δ 8.55 (s, 1H, exch.), 7.84 (d, *J* 7.1, 2H), 7.57-7.18 (m, 8H), 4.77 (t, *J* 5.3, 1H, exch.), 4.74 (brs, 1H), 3.56 (s, 3H, OMe), 3.54-3.48 (m, 2H), 3.45-3.39 (m, 1H), 3.35-3.27 (m, 1H), 2.86 (dd, *J* 15.2, 6.3, 1H), 2.75 (dd, *J* 15.2, 9.5,1H), 2.65-2.55 (m, 1H), 2.30-2.18 (m, 2H), 2.14-2.05 (m, 1H), 1.85-1.68 (m, 2H); ^{13}C NMR (DMSO-d_6, 125 MHz) δ 28.2, 31.3, 34.1, 34.6, 38.2, 51.7, 55.8, 59.9, 60.9, 125.7, 127.5 (x2), 127.9 (x4), 128.4 (x2), 131.2, 133.8, 138.6, 166.6, 173.4, 173.9; MS (ESI+) 447.3 [M+23] $C_{24}H_{28}N_2O_5$ Calcd for: C, 67.91; H, 6.65; N, 6.60; Found: C, 67.78; H, 6.80; N, 6.49.

(*S*)-**6a**: 4.1 g, 23%. Mp 230 °C dec. (CH_2Cl_2/*n*-hexane); $[\alpha]_D^{25}$ -47.7 (*c* 0.1, DMSO); ν_{max} 3435, 1737, 1627cm^{-1}; ^1H NMR (DMSO-d_6, 500 Mz) δ 8.51 (s, 1H, exch.), 7.82 (d, *J* 7.1, 2H), 7.58-7.15 (m, 8H), 4.75 (t, *J* 4.8, 1H, exch.), 4.54 (brs, 1H), 3.58 (s, 3H), 3.55-3.42 (m, 3H), 3.35-3.22 (m, 1H), 2.24-2.71 (m, 2H), 2.66 (dd, *J* 13.1, 13.6, 1H), 2.38-2.28 (m, 1H), 2.25-2.07 (m, 2H), 1.83 (dd, *J* 13.5, 12.8, 1H), 1.81-1.70 (brs, 1H); ^{13}C NMR (DMSO-d_6, 125 Mz) δ 28.2, 31.2, 34.1, 34.3, 39.1, 51.7, 57.8, 60.1, 60.9, 125.7, 127.5 (x2), 127.9 (x2), 127.9 (x2), 128.6 (x2), 131.2, 133.9, 138.8, 166.9, 173.6, 173.9; MS (ESI+) 447.2 [M+23] $C_{24}H_{28}N_2O_5$ Calcd for: C, 67.91; H, 6.65; N, 6.60; Found: C, 67.78; H, 6.80; N, 6.49.

Methyl 5-Benzoylamino-1-[(S)-2-hydroxy-1-phenylethyl]-2-oxoazepan-5-carboxylate (5b/6b): 50:50. Column chromatoghraphy condition: CH_2Cl_2/MeOH, from 100:0 to 50:1

(*R*)-5b: 5.7 g, 35% Mp 260 °C (CH_2Cl_2/MeOH); $[\alpha]_D^{25}$ +13.2 (*c* 0.2, MeOH); IR (KBr)ν_{max}3359, 1726, 1624 cm^{-1}; ^1H NMR (DMSO-d_6, 300 MHz) *δ* 8.58 (s, 1H, exch), 7.84 (d, *J* 8.2, 2H), 7.58-7.25 (m, 8H), 5.63 (t, *J* 6.8, 1H),4.93 (brs, 1H, exch), 3.88 (t, *J* 4.7, 2H), 3.54 (s, 3H), 3.56-3.54; 3.30-3.20 (2 m, 2H), 2.74 (dd, *J* 2.5, 2.0, 1H), 2.55-2.25 (m, 2H), 2.10-1.85 (m, 2H), 1.50 (br, 1H); ^{13}C NMR (DMSO-d_6, 75 Mz) *δ*29.6, 32.3, 35.5, 39.3, 52.8, 58.0, 60.6, 61.0, 128.1, 128.6 (x2), 128.7

(x2), 129.0 (x2), 129.2 (x2), 132.3, 134.9, 139.5, 167.7, 174.5, 174.9; **MS** (ESI+) 411.2 [M+1], 433.3 [M+23] $C_{23}H_{26}N_2O_5$, Calcd for: C, 67.30; H, 6.38; N, 6.82; Found: C, 67.01; H, 6.55; N, 6.63.

(*S*)-6b: (trace amount of **5b** are present); 4.9g, 30%, IR (KBr) ν_{max} 3412, 1738, 1627 cm^{-1}; ^1H NMR (DMSO-d_6, 300 MHz) δ8.49 (s, 1H, exch.), 7.85 (d, *J* 7.2, 2H.), 7.56-7.20 (m, 8H.), 5.66 (dd, *J* 13.8, 5.9, 1H), 4.93 (t, *J* 4.8, 1H, exch), 4.00-3.75 (m, 2H), 3.60 (s, 3H), 3.53 (dd, *J* 15.9, 10.1, 1H), 3.13 (dd, *J* 15.9, 6.1, 1H), 2.89 (t, *J* 13.5, 1H), 2.60-2.40 (m, 1H), 2.28 (dd, *J* 14.5, 8.3, 1H), 2.25-2.10 (m, 1H), 2.10-1.85 (m, 2H); ^{13}C NMR (DMSO-d_6, 75 MHz) δ29.1, 32.1, 35.8, 39.4, 52.9, 57.9, 60.5, 61.3, 127.9, 128.4 (x2), 128.7 (x2), 129.0 (x2), 129.2 (x2), 132.2, 135.0, 139.7, 167.9, 174.8, 175.5; MS (ESI+) 411.4 [M+1], 433.4 [M+23],$C_{23}H_{26}N_2O_5$. Calcd for: C, 67.30; H, 6.38; N, 6.82; Found: C, 66.97; H, 6.54; N, 6.58.

Methyl 7-benzoylamino-(*S*)-3-benzyl-3,5,6,7,8,9-hexahydro-oxazolo[3,2-*a*]azepinium-7-carboxylate · BF_4^- (3a/4a): 67:33.

(*R*)-**3a** (mixture with (*S*)-**4a)**: ^1H NMR ($CDCl_3$, 500 MHz) main signals: δ 7.92 (d, *J* 7.1, 2H), 4.91 (m, 1H), 4.70 (m, 1H), 4.68 (m, 1H), 4.10-4.00 (m, 1H), 3.69 (s, 3H, OMe), 2.00-1.70 (m, 2H); ^{13}C NMR ($CDCl_3$, 125 MHz) δ 23.1, 27.7, 29.7, 32.1, 36.7, 42.5, 53.1, 60.2, 65.6, 76.3, 127.6 (x2), 127.9, 128.6 (x2), 129.2 (x2), 129.4 (x2), 132.2, 132.8, 133.5, 167.9, 173.1, 179.0.

(*S*)-**4a**: ν_{max} 3400, 1738, 1661 cm^{-1}; ^1H NMR ($CDCl_3$, 500 MHz) δ 7.88 (d, *J* 7.2, 2H), 7.50-7.46 (m, 1H), 7.42-7-37 (m, 5H), 7.36-7.33(m, 1H), 7.22 (d, *J* 6.9, 2H), 5.03 (dd, *J* 9.8, 9.3, 1H), 4.97-4.90 (m, 1H), 4.68 (dd, *J* 9.3, 5.9, 1H), 3.98 (dd, *J* 15.1, 8.5, 1H), 3.81 (dd, *J* 15.1, 9.3, 1H), 3.74 (s, 3H), 3.25 (dd, *J*14.4, 5.0, 1H), 3.09 (dd, *J* 17.7, 10.3, 1H), 3.04 (dd, *J* 14.4, 7.5, 1H), 2.86 (dd, *J* 17.7, 8.8, 1H), 2.82 (dd, *J* 16.7, 9.2, 1H), 2.67 (ddd, *J* 16.3, 9.0, 1.6, 1H), 2.30-2.59 (dd, *J* 15.6, 8.3 1H), 2.54 (ddd, *J* 16.3, 13.5, 1.8, 1H); ^{13}C NMR ($CDCl_3$, 125 MHz) δ 21.9, 26.4, 31.4, 36.3, 41.8, 52.3, 59.2, 64.6, 75.5, 126.8(x2), 127.5, 127.9 (x2), 128.5 (x2), 128.8 (x2), 131.4, 132.1, 132.2, 166.9, 172.2, 178.6; MS (ESI+) 407.3 $[M]^+$ $C_{24}H_{27}N_2O_4$. Calcd for: C, 70.74; H, 6.68; N, 6.87; Found: C, 70.62; H, 6.90; N, 6.68

(*R*)-5-Benzoylamino-1-[(*S*)-1-hydroxy-3-phenylpropan-2-yl]-2-oxoazepane-5-carboxylic acid (7). Ester **5a** (300 mg, 0.7 mmol) was dissolved in CH_2Cl_2/MeOH (9:1, 10.5 mL). A methanolic

solution of NaOH (2N, 1.13 mL) was added and the mixture was stirred at 25 °C for 15 h (TLC: CH_2Cl_2/MeOH, 10:1). After solvent evaporation, the mixture was taken up with H_2O and acidified 12 N with HCl until pH 1. A solid was separated and filtered corresponding to acid **7** (220 mg). The aqueous solution was extracted with CH_2Cl_2 (3 x 3 mL). The organic layers were then dried over Na_2SO_4 and the solvent was removed under vacuum. After crystallization, a further crop of pure compound **7** was obtained (50 mg). Acid **7** (270 mg) was obtained in 95% overall yield.

Mp: 180 °C (Et_2O); $[\alpha_D]^{25}$ +18.3 (*c* 0.1, MeOH); IR (KBr) ν_{max} 3353, 2923, 1720 cm^{-1}; ^1H NMR (DMSO-d_6, 300 MHz) δ 12.28 (brs, 1H), δ 8.40 (s, 1H), 7.84 (d, *J* 7, 2H), 7.59-7.17 (m, 8H), 4.93-4.71 (m, 1H), 4.30 (brs, 1H), 3.65-3.27 (m, 4H), 2.97-2.70 (m, 2H), 2.63-2.42 (m, 1H), 2.38-2.01 (m, 3H), 1.98-1.80 (m, 2H); ^{13}C NMR (DMSO-d_6, 75 MHz) δ 29.3, 32.5, 35.2, 35.8, 42.1, 57.2, 61.9, 65.4, 126.8, 128.5(x2), 128.9(x 2), 129.0(x2), 129.5(x2), 132.1, 135.2, 139.7, 162.3, 175.1, 175.4; MS (ESI-) 409.6 [M-1]. $C_{23}H_{26}N_2O_5$ Calcd for: C, 67.30; H, 6.38; N, 6.82; Found: C, 67.13; H, 6.53; N, 7.01.

Synthesis of dipeptide 8. Benzyl ester of (*L*)-alanine *p*-toluenesulfonate (200 mg, 1.11 mmol) was suspended in CH_2Cl_2 (5 mL) and then treated with triethylamine (155 μL, 1.11 mmol). The mixture was washed with H_2O. The organic layer was dried over Na_2SO_4 and the solvent was evaporated under vacuum. Acid **7** (130 mg, 0.320 mmol) was dissolved in a mixture of CH_2Cl_2 (3.2 mL)/DMF (0.1 mL) mixture. After cooling to 0°C, HOAt (44 mg, 0.320 mmol), EDC (61 mg, 0.320 mmol), alanine benzyl ester (170 mg, 0.950 mmol) and DIPEA (2 equiv., 0.112 mL, until pH 8) were added to the mixture. The reaction was left under stirring overnight at 25 °C (TLC: CH_2Cl_2/MeOH, 10:1). The crude was washed with aqueous HCl (3N, 2 x 5 mL), H_2O (5 mL) and finally with $NaHCO_3$ (2 x 5 mL). The organic layer was dried over Na_2SO_4 and the solvent was evaporated under vacuum. The crude mixture was crystallized affording pure compound **13** (185 mg, 80%). Mp: 120 °C (CH_2Cl_2/Et_2O); $[\alpha_D]^{25}$ -27.5 (*c* 0.1, MeOH); IR (KBr) ν_{max} 3400, 1740 cm^{-1}; ^1H NMR ($CDCl_3$, 300 MHz) δ 7.77 (d, *J* 6.9, 2H), 7.48-7.14 (m, 14 H), 7.01 (s, 1H), 5.11 (q, *J* 11.9 , 2H), 4.70 (brs, 1H), 4.53 (t, *J* 14.07, 1H), 3.72-3.57 (m, 2H), 3.46-3.26 (m, 2H), 2.85-2.52 (m, 4H), 2.29-2.02 (m, 4H), 1.38-1.27 (m, 3H), 1.27 (s, 1H); ^{13}C NMR ($CDCl_3$, 75 MHz) δ 18.3, 29.3, 32.3, 35.2, 36.1, 40.9, 48.8, 59.5, 61.6, 63.1, 67.4, 127.0, 127.2, 127.4, 127.7, 128.4 128.5 (x2), 128.6, 128.7, 128.9, 129.0, 129.1, 129.3, 129.8, 132.3, 134.4, 135.7, 138.2, 168.4, 172.9, 173.1, 176.4; MS (ESI-) 570.9 [M-1]. $C_{33}H_{37}N_3O_6$ Calcd for: C, 69.33; H, 6.52; N, 7.35; Found: C, 69.57; H, 6.23; N, 7.04.

Debenzylation of ester 8. Ester **8** (100 mg, 0.175 mmol) was dissolved in MeOH (5 mL). Pd/C (185 mg, 0.175 mmol) was added and the mixture was hydrogenated at 25 °C overnight (TLC: CH_2Cl_2/MeOH, 10:1). The catalyst was filtered on a celite pad and acid **9** (75 mg, 90%) was obtained after crystallization. Mp: 140°C (CH_2Cl_2/Et_2O); $[\alpha_D]^{25}$ -20.8 (*c* 0.2, MeOH); IR (KBr) ν_{max} 3400, 2928, 1730, 1629 cm^{-1}; ^1H NMR (CD_3OD, 300 MHz) δ 7.85-7.82 (m, 2H), 7.57-7.43 (m, 3H), 7.31-7.19 (m, 5H), 4.32 (q, *J* 7.1, 1H), 3.76-3.63 (m, 2H), 3.55 (brs, 2H), 3.36-3.31 (m, 2H), 2.92-2.78 (m, 2H), 2.61-2.41 (m, 3H), 2.23-2.01 (m, 3H), 1.35 (d, *J* 7.1, 3H); ^{13}C NMR **(**CD_3OD, 75 MHz) δ 17.2, 28.3, 31.8, 34.8, 35.6, 39.8, 48.6, 49.2, 58.6, 61.6, 126.5, 127.5, 127.6, 127.7, 128.5(x2), 128.8(x2), 129.1, 131.8, 134.8, 138.5, 169.5, 174.1, 175.8, 176.8; MS (ESI+) 504.3 [M+23]. $C_{26}H_{31}N_3O_6$ Calcd. for: C, 64.85; H, 6.49; N, 8.73; Found: C, 64.56; H, 6.78; N, 8.46;

Synthesis of tetrapeptide 10. Acid **9** (60 mg, 0.125 mmol) was suspended in a mixture of CH_2Cl_2 (1.25 mL)/DMF (0.1 mL). After cooling to 0°C, HOAt (17 mg, 0.125 mmol), EDC (24 mg, 0.125 mmol), dipeptide H_2N-Aib-(*L*)-AlaNHMe (60 mg, 0.312 mmol) and DIPEA (2 equiv., 0.044 mL, until pH 8) were added to the mixture. The reaction was stirred at 25°C overnight (TLC: CH_2Cl_2/MeOH, 10:1). The mixture was washed with aqueous HCl (3N, 2 x 5 mL), H_2O (5 mL) and finally with $NaHCO_3$ (2 x 5 mL). The organic layer was dried over Na_2SO_4 and the solvent was evaporated under vacuum. The crude mixture was crystallized from CH_2Cl_2/Et_2O affording crude peptide **10** (40 mg, 50%). A further purification was performed by HPLC (phase A: 95% H_2O, 5% CH_3CN, 1 mL TFA; phase B: 95% CH_3CN, 5% H_2O, 1 mL TFA; elution gradient: 95% A for 5 min, then 95-30% A in 20 min) to give peptide **10** (20 mg, 25%). During the purification we observed the formation of a by-product, corresponding to the bicyclic derivative **11**. Alternatively, pure peptide **10** (30 mg, 38%) can be directly obtained from the crude by performing a second crystallization. Mp: 120°C (CH_2Cl_2/Et_2O); $[\alpha_D]^{25}$ +6.2 (*c* 0.2, MeOH); IR (KBr) ν_{max} 3400, 1740 cm^{-1}; ^1H NMR **(**CD_3CN, 300 MHz) δ 8.92 (s, 1H), 7.94 (d, *J* 7.2, 2H), 7.69 (brs, 1H), 7.60 (d, *J* 10.9, 1H), 7.54-7.51 (m, 3H), 7.45 (d, *J* 3.9, 1H), 7.39-7.17 (m, 7H), 4.71 (brs, 1H), 4.26-4.08 (m, 1H), 3.93-3.87 (m, 1H), 3.70-3.31 (m, 4H), 3.13-3.03 (m, 1H), 2.83-2.71 (m, 2H), 2.66 (d, *J* 4.6, 3H), 2.59-1.90 (m, 5H), 1.55-1.32 (m, 12H); ^{13}C NMR **(**CD_3CN, 75 MHz) δ 15.8, 16.9, 23.0, 25.3, 26.4, 28.5, 30.1, 31.5, 34.3, 36.5, 42.7, 49.7, 52.4, 56.6 , 62.0, 65.5, 126.1, 127.8, 128.4, 128.6, 129.1, 129.5, 130.3, 132.0, 132.3, 133.7, 134.2, 139.0, 167.8, 168.5, 173.2, 174.1, 174.5, 175.5; MS

(ESI+) 651.3 [M+1]. $C_{34}H_{46}N_6O_7$ Calcd. for: C, 62.75; H, 7.12; N, 12.91; Found: C, 62.56; H, 7.34; N, 13.17.

Synthesis of 12. Alcohol **5a** (0.26 mmol) was dissolved in CH_2Cl_2 (3 mL) and 3-tritylsulfanyl-propionic acid (100 mg, 0.286 mmol) was added. After cooling to 0°C, DMAP (3 mg, 0.026 mmol) was added and DCC (36 mg, 0.286 mmol) dissolved in CH_2Cl_2 (1 mL) was dropped to the solution. The reaction was stirred for 3h at 25 °C (TLC: CH_2Cl_2/AcOEt, 1:1). The mixture was washed with $NaHCO_3$ (5 mL) and H_2O (5 mL). The organic layer was dried over Na_2SO_4 and the solvent was evaporated under vacuum. Pure compound **12** (155 mg, 80%) was obtained after crystallization. Mp: 80°C (AcOEt/Et_2O); $[\alpha_D]^{25}$ -8.7 (*c* 0.2, MeOH); IR (KBr) ν_{max} 3326, 1738 cm^{-1}; ^1H NMR ($CDCl_3$, 200 MHz) δ 7.77-7.70 (m, 2H), 7.51-7.17 (m, 23H), 6.09 (bs, 1H), 5.01-4.76 (m, 1H), 4.74 (bs, 1 H), 4.39-4.01 (m, 2H), 3.69 (s, 3H), 3.39-3.21 (m, 3H), 2.94-2.84 (m, 2H), 2.59-2.45 (m, 2H), 2.02-1.45 (m, 6H); ^{13}C NMR ($CDCl_3$, 75 MHz) δ 24.5, 24.7, 25.5, 29.8, 33.3, 33.8, 35.3, 50.5, 52.8, 60.6, 64.3, 67.2, 126.9 (x4), 127.2(x2), 127.4(x2), 127.9, 128.1(x4), 128.4, 128.7, 128.8, 129.1, 129.2, 129.5, 129.7, 129.8(x4), 132.1, 134.0, 137.6, 144.7, 147.1, 157.8, 167.4, 171.7, 173.2, 174.9; MS (ESI+) 777.5 [M+23]. $C_{46}H_{46}N_2O_6S$ Calcd for: C, 73.18; H, 6.14; N, 3.71; Found: C, 72.91; H, 6.35; N, 3.65.

Preparation of covered gold nanoparticles. In a typical experiment **12** (0.5 mmol) and $HAuCl_4 \cdot 3H_2O$ (0.25 mmol) were combined in a 4:1 methanol/milli-Q water solvent mixture (10 ml). The resulting solution was allowed to stand at 0°C for 1 h under stirring. To this solution, a cold $NaBH_4$ (2.5 mmol) solution in MeOH (2ml) was rapidly added and the resulting mixture was stirred at room temperature for additional 4 hrs. The reaction was quenched by addition of 0.1 M HCl (1 ml). The solvent mixture was removed under reduced pressure to dryness and the dark residue was dissolved in CH_2Cl_2 (20 ml), washed with H_2O, dried over anhydrous Na_2SO_4, and evaporated to dryness. Subsequently, the crude was dissolved in MEOH, passed through a 20 μm microfilter and afterward precipitated by adding a large amount of Et_2O. Finally, the corresponding AuNp was obtained after centrifugation.

Determination of AuNp-12 conjugated structural information.

The number of Au atoms in the relative AuNps were calculated from: a) dimension of the metallic core (diameter) observed in the TEM images,b) the density of bulk metal (55 atoms/nm^3), c)

applying the sphere model. The numbers of moieties conjugated to the inorganic cluster were calculated from the TGA weight losses (corresponding to the weight fractions of the organic coating monolayer on the inorganic cluster) and the molecular weight of the related oligomers conjugated to the inorganic core. Consequently, the oligomer footprints of the different AuNps were calculated by relating the number of oligomers linked on the gold surface with the dimensional information obtained by the TEM analysis.

ASSOCIATED CONTENT

Supporting Information. A CIF file giving X-ray data for **4a**, NMR data for compounds **4a**, **10**, **11**. HPLC spectrum of pure compound **10**. ^{1}H, ^{13}C NMR spectra for all new compounds. Geometries of representative structures of peptide **10**. Amber ff99SB library for oxo-Azn **5a**. This material is available free of charge via the Internet at http://pubs.acs.org.

ACKNOWLEDGMENT

Funding for this work was provided by MIUR (PRIN 2010-2011 - prot. 2010NRREPL).

REFERENCES

(1) a) Alex, S.; Tiwari, A. *J. Nanosci. Nanotec.*, **2015**, *15*, 1869-1894 b) Yongsheng, M.; Pengxia, L.; Zhou, Y.; Dong, W.; Wanli, H.; Hui, C.; Huai, Y. *RSC Adv*., **2015**, *5*, 140-145; c). Figuero, E. R; Lina, A. Y.; Yana1, J.; Luoa, L.; Fosterb, A. E.; Drezek R. A. *Biomaterials*, **2014**, *35*, 1725–1734; d) Sapsford, K. E.; Algar, W. R.; Berti, L.; Boeneman Gemmill, K.; Casey, B. J.; Oh, E.; Stewart, M. H.; Medintz I. L. *Chem. Rev.* **2013**, *113*, 1904−2074; e) Jadhav, S. A. *J.Mater.Chem.,* **2012***, 22,* 5894*;* f) Prats-Alfonso, E.; Albericio, F. *J. Mater. Sci.,* **2011***, 46,* 7643–7648*;* g) Giljohann, D. A.; Seferos, D. S.; Daniel, W. L.; Massich; Patel, P. C.; Mirkin, C. A. *Angew. Chem., Int. Ed.*, **2010**, *49*, 3280–3294.
(2) a) Osante, I.; Polo, E.; Revilla-Lo´pez, G.; de la Fuente, J, M.; Alema´n, C.; Cativiela, C.; Dı´az, D. *J. Nanopart. Res.,* **2014**, *16*, 2224-2236; b) Srisombat, L.; Jamison, A.C.; Lee, T.R. *Colloid Surf A*, **2011**, *390,* 1–19.
(3) Panda, J. J.; Chauhan, V S. *Polym. Chem.*, **2014**, *5*, 4418-4436; b) Parween, S.; Misra, A.; Ramakumar, S.; Chauhan, V. S *J. Mater. Chem. B*, **2014**, *2*, 3096-3106; c) Montenegro, A.; Ghadiri, V; Granja, J. R. *Acc. Chem. Res.* **2013**, *46*, 2955-2965; d) Hourani, R.; Zhang, C.; van der Weegen, R.; Changyi, L. R.; Keten, L. S.; Helms, B. A.; Xud, T. *J.Am.Chem.Soc.* **2011**, *133*, 15296– 15299; e) Lalatsa, A; Schätzlein, A. G.; Mazza, M.;. Hang Le, T. B.; Uchegbue, I. F. *J. Control. Rel.* **2012**,

161, 523—553.
(4) a) Leea, E.-J.; Bea, C. L.; Vinsona, A. R., Richesa, A. G.; Fehra, F.; Gardinera, J.; Gengenbacha, T. R.; Winklera, D. A.; Haylock, D. *Biomaterials*, **2015**, *37*, 82–93; b) de Bruyn Ouboter, D.; Schuster, T. B.; Sigg, S. J.; Meier, W. P. *Colloids and Surfaces B: Biointerfaces* **2013**, *112*, 542-547.
(5) Aili, D.; Gryko, P.; Sepulveda, B.; Dick, J. A. G.; Kirby, N.; Heenan, R.; Baltzer, L.; Liedberg, B.; O Mary, P. R.; Stevens, M. M. *Nano Lett.* **2011**, *11*, 5564–5573.
(6) a) Parween, S.; Ali, A.; Chauhan, V. S *ACS Appl. Mater. Interfaces* **2013**, *5*, 6484-6493; b) Rio-Echevarria, I. M.; Tavano, R.; Causin, V.; Papini, E.; Mancin, F.; Moretto, A. *J. Am. Chem. Soc.* **2011**, *133*, 8-11; c) Aili, D.; Stevens, M. M. *Chem. Soc. Rev.*, **2010**, *39*, 3358–3370.
(7) Avan, I.; Hall, C. D.; Katritzky, A. R. *Chem. Soc. Rev.*, **2014**, *43*, 3575-3594.
(8) a) Maffucci , I.; Pellegrino, S.; Clayden, J.; Contini, A. *J. Phys. Chem. B* **2015**, *119*, 1350-1361; b) Demizu, Y.; Doi, M.; Kurihara, M.; Okuda, H.; Nagano, M.; Suemune, H.; Tanaka, M. *Org. Biomol. Chem*. **2011**, *9*, 3303–3312; c) Gatto, E.; Porchetta, A.; Stella, L.; Guryanov, I.; Formaggio, F.; Toniolo, C.; Kaptein, B.; Broxterman, Q. B.; Venanzi, M. *Chem. Biodiversity* **2008**, *5*, 1263–1278 d) Tanaka, M. *Chem. Pharm. Bull*. **2007**, *55*, 349-358; e) Toniolo, C.; Crisma, M.; Formaggio, F.; Peggion, C.; Broxterman, Q. B.; Kaptein, B. *Biopolymers* **2004**, *76*, 162–176.
(9) a) Pellegrino, S.; Contini, A.; Gelmi, M.L.; Lo Presti, L.; Soave, R.; Erba, E. *J. Org. Chem*. **2014**, *79*, 3094-3102; b) Bonetti, A.; Clerici, F.; Foschi, F.; Nava, D.; Pellegrino, S.; Penso, M.; Soave, R.; Gelmi, M.L;. *Eur. J. .Org. Chem.*, **2014**, 3203-3209 c) Pellegrino, S.; Contini, A.; Clerici, F.; Gori, A.; Nava, D.; Gelmi, M. L. *Chem. Eur. J.* **2012**, *18*, 8705-8715; d) Penso, M.; Foschi, F.; Pellegrino, S.; Testa, A.; Gelmi, M.L. *J. .Org. Chem.*, **2012**, *77*, 3454-3461; e) Gassa, F.; Contini, A.; Fontana, G.; Pellegrino, S.; Gelmi, M.L. *J. Org. Chem*. **2010**, *75*, 7099-7106; f) S. Pellegrino, F. Clerici, M. L. Gelmi *Tetrahedron* **2008**, *64,* 5657-5665; g) Cabrele, C.; Clerici, F.; Gandolfi, R.; Gelmi, M.L.; Molinari, F.; Pellegrino, S. *Tetrahedron*, **2006**, *62*, 3502-3508; h) Ruffoni, A.; Contini, A.; Soave, R.; Lo Presti, L.; Esposto, I.; Maffucci, I.; Nava, D.; Pellegrino, S.; Gelmi, M.L.; Clerici, F. *RSC Adv.*, **2015**, *5*, 32643-32656.
(10) a) Ribelin, T.; Katz, C. E Withrow, D.; Smith, S.; Manukyan, A.; Day, V. W.; Neuenswander,B.; Poutsma, J. L.; Aubé, J. *Angew Chem, Int Ed* **2008**; *47*, 6233–6235; b) Katz, C. E.; Ribelin, T.; Withrow, D.; Basseri, Y.; Manukyan, A. K.; Bermudez, A.; Nuera, C. G.; Day, V. W.; Powell, D. R.; Poutsma, J. L.; Aubé, J. *J. Org. Chem.* **2008**, 73, 3318-3327; c) Katz, C. E; Aubé, J. *J. Am.. Chem. Soc.* **2003**, *125*, 13948-13949; d) Sahasrabudhe, K.; Gracias, V.; Furness, K.; Smith, B. T.; Katz, C. E.; Reddy, D. S.; Aubé, J. *J. Am. Chem. Soc.,* **2003**, *125*, 7914-7922; e) Gracias, V.; Frank, K.E., Milligan, G. L.; Aubé, J. *Tetrahedron*, **1997**, *53*, 16241-16252; f) Gracias, V.; Milligan, G. L.; Aubé, J. *J. Am. Chem. Soc.*, **1995**, *117*, 8047-8048.
(11) a) Jung, G.; Bruckner, H.; Bosch, R.; Winter, V.; Schaal, H.; Strahle, J. *Liebigs Ann. Chem*. **1983**, 7, 1096-1106; b) Francis, A. K.; Iqbal, M.; Balaram, P.; Vijayan, M. *Biopolymers* **1983***, 22*, 1499-1505; c) Leibfritz, D.; Brunne, R. M.; Weihrauch, T.; Stelten, J.; Stohrer, W.-D.; Haupt, E. T. K *Liebigs Ann. Chem*., **1989**, *13*, 1017–1027; d) Schweitzer-Stenner, R.; Gonzales , W.; Bourne, G. T.; Feng, J. A.; Marshall, G. R. *J. Am. Chem. Soc.* **2007**, *129*, 13095-13109 and references cited therein; e) Longo, E.; Moretto, A.; Formaggio, F.; Toniolo, C. *Chirality*, **2011***, 23*, 756-760 and reference cited therein
(12) a) Nuñez-Villanueva, D.; Infantes, L.; García-Lopez, M. T.; Gonzaĺez-Muñiz, R.; Martín-Martínez, M. *J. Org. Chem.* **2012**, *77*, 9833-9839; b) Nuñez-Villanueva, D.; Infantes, L.; García-Lopez, M. T.; Gonzaĺez-Muñiz, R. *J. Org. Chem.* **2011**, *76*, 6592–6603.
(13) An exception involved the terminal Ala4, that show a widened φ (averagely about -85 deg.) and a positive average ψ, although characterized by a high standard deviation which might mean a difficulty in the clusterization process, possibly due to an higher conformational variability of the

C-terminal region respect to the remaining peptide.
(14) a) Alvarez, M. M.; Khoury, J. T.; Schaaff, T. G.; Shafigullin, M. N.; Vezmar, I.; Whetten, R. L. *J. Phys. Chem. B* **1997**, *101*, 3706-3712; b) G. Mie, *Ann. Phys.* **1908**, *25*, 377-445; c) Kreibig, U. ; Genzel, L. *Surf. Sci.*, **1985**, *156*, 678-700; d) Quinten, M.; Kreibig, U. *Surf. Sci.* **1986**, *172*, 557-577; e) Barnett, R. N.; Cleveland, C. L.; Häkkinen, H.; Luedtke, W. D.; Yannouleas, C.; Landman, U. *Eur. Phys. J. D* **1999**, *9*, 95-104; f) Kelly, K. L.; Coronado, E. L. L.; Schatz, G. C. *J. Phys. Chem. B* **2003**, *107*, 668-677.
(15) a) Gautier, C.; Bürgi, T. *J. Am. Chem. Soc.*, **2006**, *128*, 11079–11087; b) Longo, E.; Orlandin, A.; Mancin, F.; Scrimin, P.; Moretto, A. *ACS Nano*, **2013**, *11*, 9933-9939.
(16) Knoppe, S.; Dolamic, I.; Dass, A.; Bürgi, T.. *Angew. Chem. Int. Ed.* **2012**, *51*, 7589-7591.
(17) MOE *Molecular Operating Environment (MOE)*, 2013.08; Chemical Computing Group Inc.: 1010 Sherbooke St. West, Suite #910, Montreal, QC, Canada, H3A 2R7, 2013.
(18) Dupradeau, F.-Y.; Pigache, A.; Zaffran, T.; Savineau, C.; Lelong, R.; Grivel, N.; Lelong, D.; Rosanski, W.; Cieplak, P., *Phys. Chem. Chem. Phys.* **2010,** *12* (28), 7821-7839.
(19) Hornak, V.; Abel, R.; Okur, A.; Strockbine, B.; Roitberg, A.; Simmerling, C., *Proteins: Struct., Funct., Bioinf.* **2006,** *65* (3), 712-725.
(20) Case, D.A.; Babin, V.; Berryman, J.T.; Betz, R.M.; Cai, Q.; Cerutti, D.S.; Cheatham, T.E. III; Darden, T.A.; Duke, R.E.; Gohlke, H.; Goetz, A.W.; Gusarov, S.; Homeyer, N.; Janowski, P.; Kaus, J.; Kolossváry, I.; Kovalenko, A.; Lee, T.S.; LeGrand, S.; Luchko, T.; Luo, R.; Madej, B.; Merz, K.M.; Paesani, F.; Roe, D.R.; Roitberg, A.; Sagui, C.; Salomon-Ferrer, R.; Seabra, G.; Simmerling, C.L.; Smith, W.; Swails, J.; Walker, R.C.; Wang, J.; Wolf, R.M.; Wu, X.; Kollman, P.A. (2014), AMBER 14, University of California, San Francisco.
(21) Onufriev, A.; Bashford, D.; Case, D. A., *Proteins Struct. Funct. Bioinf.* **2004,** *55*, 383-394.
(22) Humphrey, W.; Dalke, A.; Schulten, K., *J. Mol. Graphics Modell.* **1996,** *14*, 33-38.
(23) Kabsch, W.; Sander, C., *Biopolymers* **1983,** *22* , 2577-2637.

For Table of Contents Only